J. Magn. Soc. Jpn., **41**, 58-62 (2017)

<Paper>

Morphology and magnetic properties of α"-$Fe_{16}N_2$ nanoparticles synthesized from iron hydroxide and iron oxides

M. Tobise, T. Ogawa, and S. Saito

Department of Electronic Engineering, Graduate School of Engineering, Tohoku University,

6–6–05, Aza–Aoba, Aramaki, Aoba–ku, Sendai 980–8579, Japan

Metastable α"-$Fe_{16}N_2$ have attracted much interest as a candidate for rare-earth-free hard magnetic materials. To realize high coercivity, it is necessary to utilize not only the magnetocrystalline anisotropy but also the shape anisotropy of α"-$Fe_{16}N_2$ nanoparticles assemblies. An increase in magnetostatic couplings and intergranular exchange couplings among particles typically reduces the coercivity. Therefore, it is very important to evaluate the anisotropy and magnetic interactions among α"-$Fe_{16}N_2$ nanoparticles. We have examined the changes in morphology, structure and magnetic properties through the synthesis of α"-$Fe_{16}N_2$ nanoparticles from various materials such as α-FeOOH, ɤ-Fe_2O_3, and Fe_3O_4. The magnetic interactions were also estimated based on experimental results obtained by analysis of the rotational hysteresis loss of randomly oriented nanoparticles. H_c and H_k^{ptc} for the α"-$Fe_{16}N_2$ nanoparticle assemblies for different starting materials ranged from 2.2 to 1.1 kOe, and from 11 to 12 kOe respectively. Experimental results of the normalized coercive force and normalized switching field suggests that the existence of large magnetic interactions among α"-$Fe_{16}N_2$ nanoparticles.

Key words: nanomagnetics, hard magnetic materials, iron nitride, magnetic anisotropy, rare earth element-free

1. Introduction

The metastable α"-$Fe_{16}N_2$ iron nitride phase with body-centered tetragonal (b.c.t.) structure has received much attention as a candidate for rare-earth-free hard magnetic materials. After a surprising first report where the α"-$Fe_{16}N_2$ phase exhibited giant saturation magnetization as a thin film[1], many researches have attempted to produce single phase α"-$Fe_{16}N_2$[2,3]. In 1993, a thin film method was established to achieve a relatively high volume fraction of α"-$Fe_{16}N_2$ using reactive sputtering, where a saturation magnetization of $M_s \simeq 240$ emu/g and uniaxial magnetocrystalline anisotropy constant of $K_u \simeq 1\times10^7$ erg/cm^3 were determined[4]. These values are very attractive with respect to the realization of a permanent magnet based on this material. Since it is still very difficult to produce metastable α"-$Fe_{16}N_2$ in thin films, the synthesis of single phase α"-$Fe_{16}N_2$ in bulk form is considered to be extremely challenging[5,6,7]. In 2013, a procedure for the synthesis of single phase α"-$Fe_{16}N_2$ nanoparticles was established, and α"-$Fe_{16}N_2$ was reported[8] to exhibit $M_s \simeq 226$ emu/g and $K_u \simeq 9.6\times10^6$ erg/cm^3 at 300 K.

To produce a hard magnetic material using magnetic particle, it is necessary to control the anisotropy of particle assemblies and the magnetic interaction among these particles. Magnetostatic couplings and intergranular exchange couplings among particles typically reduce the coercivity. Therefore it is very important to evaluate these magnetic interactions among α"-$Fe_{16}N_2$ nanoparticles. In this work, we examine the changes in the morphology, structure and magnetic properties of α"-$Fe_{16}N_2$ nanoparticles synthesized using different starting materials, such as α-FeOOH, ɤ-Fe_2O_3, and Fe_3O_4. We also discuss the magnetic anisotropy and magnetic interactions based on the experimental results obtained by the rotational hysteresis loss analysis[9] of randomly oriented nanoparticles.

2. Experimental Procedure

The synthesis of α"-$Fe_{16}N_2$ nanoparticles was conducted using commercially available α-FeOOH (Wako Pure Chemical Industries, Ltd.), ɤ-Fe_2O_3 (CIK NanoTek Corporation) and Fe_3O_4 (Mitsui Mining & Smelting Co., Ltd.). The diameters of the iron hydroxide and iron oxide particles ranged from several tens to several hundreds of nanometers. The temperature and duration for reduction and nitriding were systematically examined to obtain almost single phase α"-$Fe_{16}N_2$, according to the following procedure. α-FeOOH, ɤ-Fe_2O_3, and Fe_3O_4 nanoparticles were first reduced at 250−600 °C for 1−5 h in a H_2 gas flow. Nitriding was subsequently performed at 100−200 °C for 2−72 h in an NH_3 gas flow. Crystal structure analysis was conducted using powder X-ray diffraction (XRD) with CoKα radiation. Morphological changes were observed using transmission electron microscopy (TEM). For magnetic properties measurements, α-Fe and α"-$Fe_{16}N_2$ nanoparticles were packed into a disk shape (6 mm diameter, 1 mm thick) with resin. The magnetization σ, and coercivity H_c, were measured using vibrating sample magnetometer (VSM) with a maximum applied magnetic field of 14.5 kOe at 300 K.

3. Results and Discussions

3.1 Morphological and structural changes of nanoparticles prepared from various starting materials

Fig. 1 shows TEM images of α-FeOOH as a starting material, α-Fe produced by the reduction of α-FeOOH, and α”-$Fe_{16}N_2$ formed by the nitriding of α-Fe. The shape of the Fe hydroxide particles is spindle-like. Reduction was performed in an atmosphere of flowing H_2 at 380 °C for 4 h, and produced aggregates of nanoparticles by sintering. Subsequent nitriding was performed in an atmosphere of flowing NH_3 at 160 °C for 8 h. No morphological differences were observed between the reduced α-Fe and nitrided α”-$Fe_{16}N_2$ nanoparticle assemblies.

Fig. 2 shows TEM images of the ɤ-Fe_2O_3 starting material, α-Fe reduced from ɤ-Fe_2O_3 and α”-$Fe_{16}N_2$ as the nitriding product from α-Fe. The shape of the ɤ-Fe_2O_3 particles is spherical. Reduction was conducted in an atmosphere of flowing H_2 at 300 °C for 4 h. The reduction process caused the nanoparticles to form aggregates by sintering, as with the α-FeOOH starting material. Nitriding was performed in an atmosphere of flowing NH_3 at 145 °C for 8 h. The nitriding process did not result in any morphological changes, in the same way that no changes were observed with the α-FeOOH starting material.

Fig. 3 shows TEM images of the Fe_3O_4 starting material, α-Fe reduced from Fe_3O_4, and α”-$Fe_{16}N_2$ by the nitriding of α-Fe. The shape of the Fe_3O_4 particles is cubic. Reduction was performed in an atmosphere of flowing H_2 at 340 °C for 4 h. The reduction and nitriding processes did not generate any obvious macroscopic morphological changes, in contrast to that observed with the α-FeOOH and ɤ-Fe_2O_3 starting materials.

Fig. 4 shows representative XRD patterns of the α”-$Fe_{16}N_2$ nanoparticles produced from various starting materials. In the case of α”-$Fe_{16}N_2$ nanoparticles produced from α-FeOOH, ɤ-Fe_2O_3, all X-ray diffracted

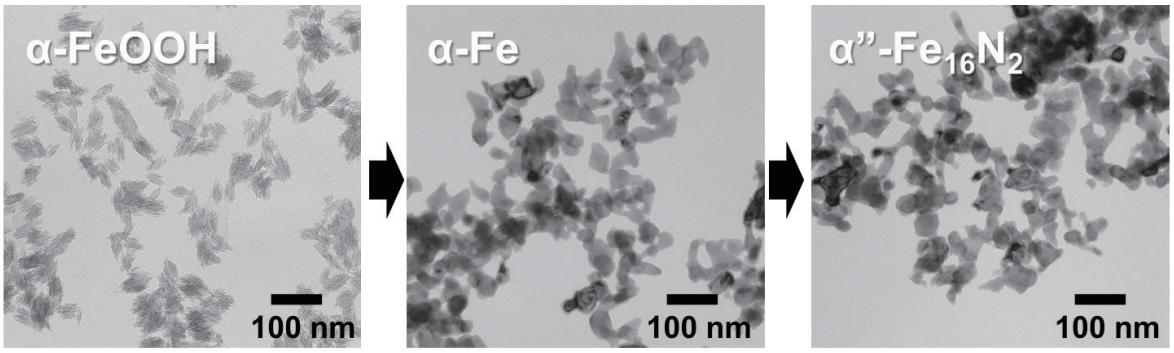

Fig.1 TEM images of α-Fe and α”-$Fe_{16}N_2$ produced from α-FeOOH as a starting material.

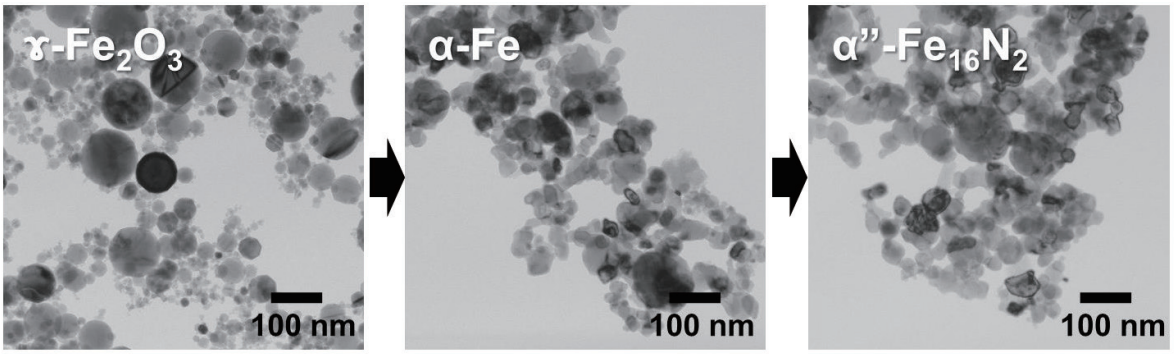

Fig. 2 TEM images of α-Fe and α”-$Fe_{16}N_2$ produced from ɤ-Fe_2O_3 as a starting material.

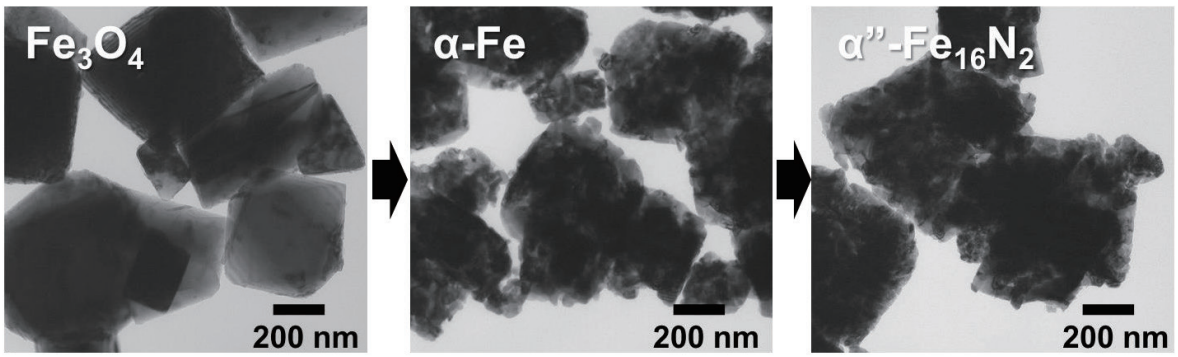

Fig. 3 TEM images of α-Fe and α”-$Fe_{16}N_2$ produced from Fe_3O_4 as a starting material.

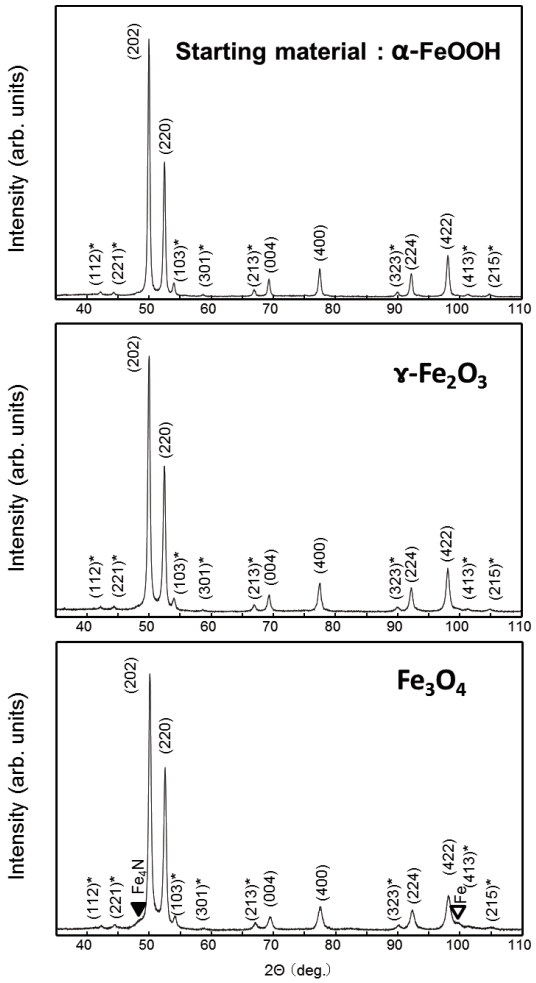

Fig. 4 XRD patterns of the α"-$Fe_{16}N_2$ nanoparticles produced from various starting materials. Asterisks show super-lattice diffraction of N ordered site.

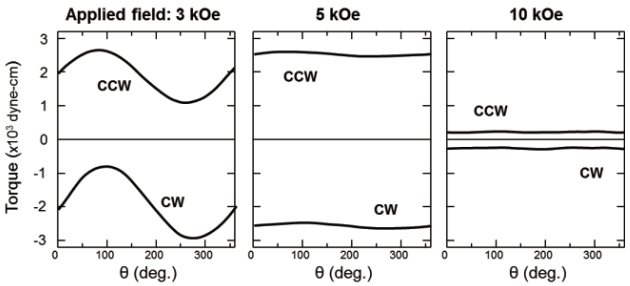

Fig. 5 Torque loss curves of α"-$Fe_{16}N_2$ randomly oriented particle assemblies produced from α-FeOOH changing applying field. CW indicates clockwise rotation and CCW indicates counter-clockwise rotation.

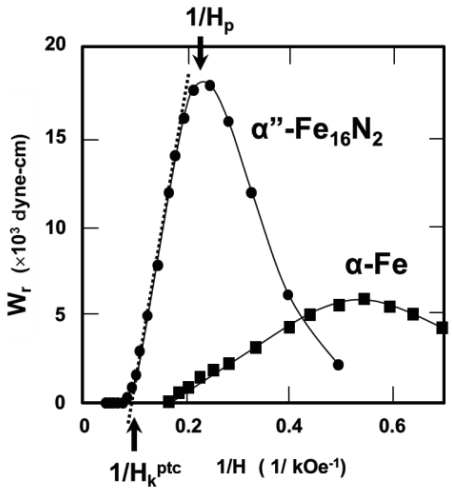

Fig. 6 Rotational hysteresis loss curves of α-Fe and α"-$Fe_{16}N_2$ nanoparticles assemblies produced from α-FeOOH.

line were identified as α"-$Fe_{16}N_2$. On the other hand, very small diffracted line besides diffractions of α"-$Fe_{16}N_2$ observed at diffraction angles around 48 and 99 degrees for α"-$Fe_{16}N_2$ nanoparticles produced from Fe_3O_4. It is supposed that these additional diffracted line correspond Fe_4N and α-Fe, respectively.

3.2 Shape anisotropy with respect to the agglomeration of nanoparticles

Fig. 5 shows the torque loss curves of α"-$Fe_{16}N_2$ randomly oriented particle assemblies produced from α-FeOOH changing applying field from 3 to 10 kOe. Rotational hysteresis loss W_r is measured as the region of enclosed area by these clockwise and counterclockwise torque curves. In the case of applying magnetic field H is larger than the half of anisotropy field H_k and smaller than H_k for the randomly oriented particles, rotational hysteresis loss W_r is observed and W_r changes as a function of magnetic field[9]. Fig. 6 shows rotational hysteresis loss curves of α-Fe and α"-$Fe_{16}N_2$ nanoparticles assemblies produced from α-FeOOH. H_k^{ptc} was defined by plotting W_r versus inverse applied field and finding the intercept by linearly extrapolating to zero hysteresis loss. H_p is the magnetic field where W_r reaches its maximum which corresponds to the switching field of assemblies of nanoparticles. H_k^{ptc} and H_p were evaluated with applying magnetic field up to 15 kOe. In the case of assemblies of particles which were magnetically isolated ideally, the value of magnetic field where W_r vanishes is independent of particle alignment (crystallographic orientation) and corresponds to H_k^{ptc}. Similar rotational hysteresis loss analysis had been already applied to the thin film recording media[10,11].

Table 1 shows the magnetic properties of α-Fe and α"-$Fe_{16}N_2$ nanoparticle assemblies produced from the different starting materials, as measured with the VSM and torque magnetometer. M_s for the α-Fe nanoparticle assemblies ranged from 205 to 198 emu/g according to the starting material. Compared to the literature value of the magnetization 218 emu/g for α-Fe, these values are lower from 6 to 9 % than the literature value. It is assumed that oxidation of surface of the α-Fe nanoparticles may cause this decrease in magnetization. H_c for the α-Fe nanoparticle assemblies ranged from 0.8 to 0.3 kOe according to the starting material, and H_k^{ptc}

Table 1. Magnetic properties of α-Fe and α"-$Fe_{16}N_2$ nanoparticle assemblies produced from various starting materials.

	α-Fe			α"-$Fe_{16}N_2$		
Starting material	α-FeOOH	ɤ-Fe_2O_3	Fe_3O_4	α-FeOOH	ɤ-Fe_2O_3	Fe_3O_4
M_s (emu/g)	205	203	198	226	192	180
H_c (kOe)	0.8	0.6	0.3	2.2	1.9	1.1
H_p (kOe)	2.0	1.7	1.3	4.2	3.8	3.0
H_k^{ptc} (kOe)	5.4	6.8	7.2	12.0	11.0	11.3
ΔN^{ptc}	3.3	4.3	4.6	——	——	——
Aspect ratio * - ellipsoid -	2.2	3.0	3.5	——	——	——

* Equivalent aspect ratio as nanoparticle assemblies

for the α-Fe nanoparticle assemblies also ranged from 5.4 to 7.2 kOe. For α-Fe nanoparticle assemblies, the anisotropy field H_k^{ptc} is considered to be due to the shape anisotropy of the nanoparticle assemblies because the magnetocrystalline anisotropy constant K_1 for α-Fe with cubic symmetry is too small (ca. 1×10^5 erg/cm^3). It is considered that the differences of H_k^{ptc} are derived from the difference of shape anisotropy in the assemblies of α-Fe nanoparticles that are formed during the reduction process. H_c for the α-Fe nanoparticle assemblies decreased from 0.8 to 0.3 kOe even though H_k^{ptc} of them increased from 5.4 to 7.2 kOe. It is assumed that H_c is not determined by only shape anisotropy. Further detailed investigation is necessary to reveal the factor which affects H_c of α-Fe.

Shape anisotropy is expressed as $K_u^{shape} = \Delta N \cdot M_s^2/2$ (or $H_k^{shape}=\Delta N \cdot M_s$). ΔN is the difference of the demagnetization coefficients between the long and short axes of a particle. The experimentally determined H_k^{ptc} was used to estimate ΔN^{ptc} as an equivalent demagnetization coefficients as nanoparticle assemblies. Fig. 7 shows an example of the calculated result[12] for

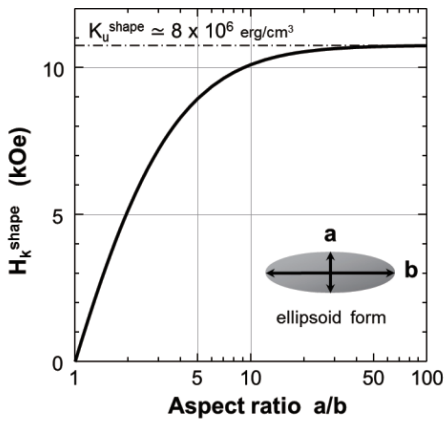

Fig. 7 Shape anisotropy field as a function of the aspect ratio for the ellipsoid form.

H_k^{shape} as a function of the aspect ratio, assuming an ellipsoid form and that the M_s of α-Fe is 218 emu/g. In this way, the values of ΔN^{ptc} were determined to range from 3.3 to 4.6 for the corresponding aspect ratios of α-Fe nanoparticle assemblies estimated with this scheme, from 2.2 to 3.5. As shown in Fig. 7, the maximum shape anisotropy is expected to be 8×10^6 erg/cm^3 with a high aspect ratio of more than 50 which is considered to be very difficult to realize.

On the other hand, H_c for the α"-$Fe_{16}N_2$ nanoparticle assemblies ranged from 2.2 to 1.1 kOe for different starting materials. The reason why that H_c of α"-$Fe_{16}N_2$ nanoparticles which were produced from Fe_3O_4 is lower than those of α"-$Fe_{16}N_2$ nanoparticles which were produced from α-FeOOH and ɤ-Fe_2O_3 is considered due to the additional α-Fe which was observed in X-ray diffraction(Fig. 4). H_k^{ptc} for the α"-$Fe_{16}N_2$ nanoparticle assemblies were not significantly different, ranging from 11 to 12 kOe. The magnetocrystalline anisotropy field H_k^{int} of α"-$Fe_{16}N_2$ determined for a pseudo single-crystalline film was 11.2 kOe[13]. This H_k^{ptc} for the α"-$Fe_{16}N_2$ nanoparticle assemblies are almost equal to H_k^{int}. If we assume α"-$Fe_{16}N_2$ nanoparticle assemblies have the same magnetocrystalline anisotropy field H_k^{int} of a pseudo single-crystalline film, the shape anisotropy is considered to be very small in α"-$Fe_{16}N_2$ nanoparticle assemblies.

3.3 Evaluation of magnetic interaction among α"-$Fe_{16}N_2$ nanoparticle assemblies

Fig. 8 shows plots of the normalized coercive force (H_c/H_k^{ptc}) versus normalized switching field (H_p/H_k^{ptc}) for α"-$Fe_{16}N_2$ nanoparticle assemblies produced from the various starting materials. H_c/H_k^{ptc} varied from 0.10 to 0.26 and H_p/H_k^{ptc} varied from 0.26 to 0.35. In the ideal magnetization reversal mode due to the coherent rotation of the magnetic moment with nonmagnetic interaction (Stoner-Wohlfarth type)[14] , H_c/H_k^{ptc} is equal to 0.48 and H_p/H_k^{ptc} is equal to 0.51. According to the micromagnetic simulation, and it was demonstrated

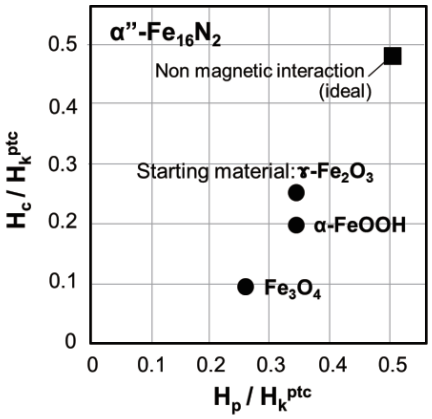

Fig. 8 Plots of H_c/H_k^{ptc} and H_p/H_k^{ptc} for α"-$Fe_{16}N_2$ nanoparticles prepared from various starting materials.

that both H_c and H_p decrease with increasing magnetic interaction among grains in thin film media[11]. Compared to the ideal values of H_c/H_k^{ptc} and H_p/H_k^{ptc}, these values of α"-$Fe_{16}N_2$ nanoparticles prepared from various starting materials are relatively small. To increase the coercivity of α"-$Fe_{16}N_2$ nanoparticles, it is necessary to decrease magnetic interaction.

3.4 Toward an increase in the coercivity of α"-$Fe_{16}N_2$ nanoparticle assemblies

The empirical figure known as the magnetic hardness parameter $\kappa = (K_1/\mu_0 M_s^2)^{1/2}$ is a useful parameter to consider how to approach the construction of modern permanent magnet[15]. The κ value for $Nd_2Fe_{14}B$ as a typical modern magnet, is 1.54, while that for α"-$Fe_{16}N_2$ is 0.53. It is recommended that κ be greater than 1, which corresponds to a value of $K_1 \simeq 3\times10^7$ erg/cm^3, assuming the same magnetization of $Nd_2Fe_{14}B$, 165 emu/g. The expected shape anisotropy is in the order of 10^6 erg/cm^3 for α"-$Fe_{16}N_2$ nanoparticles even though a high aspect ratio is realized (Fig. 7); therefor, magnetocrystalline anisotropy in the order of 10^7 erg/cm^3 is still required, in addition to improvement of the magnetic isolation among nanoparticles, for application as a permanent magnets.

4. Conclusion

The structural and magnetic properties of α"-$Fe_{16}N_2$ nanoparticles synthesized from different starting materials were examined, and the magnetic anisotropy of nanoparticle assemblies and magnetic interactions among nanoparticles were evaluated by rotational hysteresis loss analysis.

1. α-Fe nanoparticle assemblies produced by reduction and nitriding of different starting materials show exhibited different values of H_k^{ptc} ranging from 5.4 to 7.2 kOe. It is considered that the differences of H_k^{ptc} are derived from the difference of shape anisotropy in the assemblies of α-Fe nanoparticles that are formed during the reduction process. From these H_k^{ptc} values, the aspect ratio of α-Fe nanoparticle assemblies were estimated to be in the range of 2.2－3.5.

2. H_c for the α"-$Fe_{16}N_2$ nanoparticle assemblies ranged 2.2 to 1.1 kOe for different starting materials. H_k^{ptc} for the α"-$Fe_{16}N_2$ nanoparticle assemblies were not significantly different, ranging from 11 to 12 kOe.

3. The normalized coercive force (H_c/H_k^{ptc}) and normalized switching field (H_p/H_k^{ptc}) are 0.10－0.26 and 0.26－0.35 respectively, which indicates large magnetic interactions.

4. As the expected shape anisotropy is in the order of 10^6 erg/cm^3 for α"-$Fe_{16}N_2$ nanoparticles even though a high aspect ratio is realized, magnetocrystalline anisotropy on the order of 10^7 erg/cm^3 is still required, in addition to improvement of the magnetic isolation among nanoparticles to realize a permanent magnet.

Acknowledgements This work was partially supported by the New Energy and Industrial Technology Development Organization (NEDO), the Matching Planner Program from the Japan Science and Technology Agency (JST) and the Technology Research Association of Magnetic Materials for High-Efficiency Motors (MagHEM).

References

1) T. K. Kim, M. Takahashi: *Appl. Phys. Lett.*, **20**, 492 (1972)
2) J. M. D. Coey, K. O'Donnell, Q. Qinian, E. Touchais, K. H. Jack: *J. Phys.: Condens. Matter*, **6**, L23 (1994).
3) M. Komuro, Y. Kozono, M. Hanazono, and Y. Sugita: *J. Appl. Phys*, **67**, 5126 (1990)
4) M. Takahashi, H. Shoji, H. Takahashi, T. Wakiyama: *IEEE Trans. Magn.*, **29**, 3040 (1993).
5) M. Takahashi, H. Shoji: *J. Magn. Magn. Mater.* **208**, 145 (2000).
6) E. Kita, K. Shibata, H. Yanagihara, Y. Sasaki, M. Kishimoto: *J. Magn. Magn. Mater.*, **310**, 2411 (2007).
7) S. Kikkawa, A. Yamada, Y. Masubuchi, T. Takeda: *Mater. Res. Bull.*, **43**, 3352 (2008).
8) T. Ogawa, Y. Ogata, R Gallage, N. Kobayashi, N Hayashi, Y Kusano, S. Yamamoto, K. Kohara, M. Doi, M. Takano, M Takahashi: *Appl. Phys. Expres*s, **6**, 073007 (2013).
9) I. S. Jacobs, F. E. Luborsky: *J. Appl. Phys.*, **28**, 467 (1957).
10) M. Takahashi, T. Shimatsu, M. Suekane, M. Miyamura, K. Yamaguchi, H. Yamasaki: *IEEE Trans. Magn.*, **28**, 3285 (1992).
11) I. A. Beardsley and V.S. Speriosu: *IEEE Trans. Magn.*, **26**, 2718 (1990).
12) R. C. O'Handley, *Modern Magnetic Materials: Principle and Applications,* 1st ed. (John Wiley & Sons, Inc., New York, 1999), pp.38-43.
13) M. Takahashi, Y. Takahashi, K. Sunaga, H. Shoji: *J. Magn. Magn. Mater.*, **239**, 479 (2002).
14) E. C. Stoner, E. P. A. Wohlfarth: *Phil. Trans. R. Soc. Lond.*, **A 240**, 599 (1948).
15) R. Skomski, J. M. D. Coey: *Scripta Materialia*, **112**, 3 (2016)

Received Sep. 28, 2016; Revised Dec. 19, 2016; Accepted Mar. 08, 2017